A π-Configuration Plasmonic Dual Surface Plasmon Resonance Fibre Optic Sensor for Multi-Analyte Detection

Radhakrishna Prabhu * , John Ehiabhili , Somasundar Kannan

Posted Date: 30 March 2026

doi: 10.20944/preprints202603.2389.v1

Keywords: urface plasmon resonance; π-configuration; multi-analyte detection; metallic thin films; titanium dioxide (TiO_2); refractive index sensing

 doi:10.20944/preprints202603.2389.v1

Article

A π-Configuration Plasmonic Dual Surface Plasmon Resonance Fibre Optic Sensor for Multi-Analyte Detection

John Ehiabhili, Radhakrishna Prabhu * and Somasundar Kannan

School of Computing and Engineering Technology, Robert Gordon University, Aberdeen AB10 7GJ, UK

* Correspondence: r.prabhu@rgu.ac.uk; Tel.: +44-1224262252

Abstract

Although optical fibre-based surface plasmon resonance (SPR) sensors have revolutionized real-time, label-free biosensing, conventional designs suffer from limited multi-analyte detection capabilities. This study utilizes the novel Pi (π)-configured dual-SPR optical fibre sensor with two opposing side-polished surfaces, enabling plasmonic excitation for simultaneous multi-analyte detection. The proposed sensor leverages asymmetric metallic thin films such as Ag, Au, Cu and hybrid configurations (metal + TiO_2) to generate two distinct resonance peaks, significantly enhancing detection versatility. Numerical simulations using finite element method in COMSOL Multiphysics v6.3 demonstrate that the π-configuration achieves dual resonance dips at 982 nm and 1276 nm for Ag and Ag-TiO_2 films, 1040 nm and 1317 nm for Au and Au-TiO_2 films, and 977 nm and 1249 nm for Cu and Cu-TiO_2 films respectively for an analyte refractive index of 1.42. A peak spectral separation >125 nm was achieved for all the sensors for a refractive index range of 1.37 – 1.42, ensuring that the two dips are resolvable since the change in SPR wavelength is greater than or equal to the full width at half maximum, preserving dual-analyte capability and minimizing potential crosstalk. Results indicate that the π-configured dual-SPR sensor utilizing silver and silver-TiO_2 sensing layers had the highest wavelength sensitivity of 12,600 $nmRIU^{-1}$ and 20,000 $nmRIU^{-1}$ respectively, slightly outperforming its gold and copper counterpart. The optimized metallic and hybrid nanostructured films ensures dual distinct peaks with high sensitivity, while maximizing refractive index resolution. This work presents the design of a π-configured SPR-based optical fibre sensor utilizing dielectric and multi-metallic thin films, thereby offering a breakthrough in multiplexed biosensing for applications in medical diagnostics, environmental monitoring, and chemical detection.

Keywords: surface plasmon resonance; π-configuration; multi-analyte detection; metallic thin films; titanium dioxide (TiO_2); refractive index sensing

1. Introduction

Surface plasmon resonance (SPR) sensors have emerged as a cornerstone of modern optical biosensing due to their label-free, real-time, specificity, and ultra-sensitive detection capabilities [1]. These sensors exploit the excitation of surface plasmon polaritons (SPPs) at the interface between a metal (typically gold or silver) and a dielectric medium, which is highly sensitive to changes in the refractive index (RI) of the surrounding medium [2]. The resonance condition is highly dependent on the optical properties of the metal film, the incident light wavelength, and the dielectric environment, making SPR an ideal platform for detecting biomolecular interactions, chemical analytes, and environmental pollutants [3]. Conventional Kretschmann prism-based SPR sensors have been widely used, but their bulky optics and high cost limit their applicability in point-of-care diagnostics and portable sensing systems [4]. In contrast, fibre-optic SPR sensors offer a compact, flexible, and cost-effective alternative, with the added advantage of remote sensing capabilities [5,6]. Among these, D-shaped optical fibre SPR sensors have gained significant attention due to their enhanced evanescent

 doi:10.20944/preprints202603.2389.v1

field interaction resulting from side-polishing the fibre cladding, thereby improving sensitivity and detection limits [7]. Despite their advantages, conventional D-shaped SPR sensors suffer from two major limitations: generation of only one resonance peak by most fibre SPR sensors, restricting their use to single-analyte detection, and limited sensitivity and cross-talk issues in multiplexed sensing: While some multi-analyte SPR sensors have been developed using spatial multiplexing (e.g., sensor arrays) [8] or wavelength/angular interrogation [9], these approaches require complex instrumentation, increasing cost and reducing robustness.

Recent attempts to enable multi-peak SPR sensing have included tilted fibre Bragg gratings (TFBGs) [10] – but these suffer from fabrication complexity, multi-core fibres [11] – which introduce crosstalk and signal interference, and bimetallic coatings e.g., Au-Ag [12] – but these still produce overlapping resonances unless carefully optimized. Thus, there remains a critical need for a simple, high-performance SPR sensor capable of generating two or more distinct resonance peaks for multi-analyte detection. To address these challenges, we propose a novel π-configured SPR-based optical fibre sensor [13], where two opposing side-polished surfaces are functionalized with asymmetric metallic and hybrid nanostructured thin films to generate two distinct resonance peaks. The key innovations of this work include dual-SPR sensor in π-configuration, optimized bimetallic and hybrid thin-film configurations, and COMSOL Multiphysics optimized design for minimal potential crosstalk and enhanced sensitivity.

Unlike traditional single D-shaped SPR sensors, our design features two polished surfaces on opposite sides of the fibre, enabling independent plasmonic excitation at two distinct locations. This dual-sensing architecture allows for simultaneous detection of two different analytes with minimal cross-interference. We first investigate identical metal films (Ag-Ag, Au-Au, Cu-Cu) to establish baseline performance. Next, we introduce hybrid configurations (e.g., Ag on one side and Ag-TiO_2 on the other) to engineer two spectrally separated resonance dips. Titanium dioxide (TiO_2) is selected due to its high refractive index (n ≈ 2.4–2.6), which enhances the RI contrast and plasmonic field confinement, leading to sharper resonance peaks [14]. A full-wave electromagnetic simulation is performed to analyse the electric field distribution, resonance wavelength shifts, and sensitivity for different thin-film configurations. The optimal metal thicknesses (Ag/Au/Cu: 45 nm, TiO_2: 10 nm) [15,16] are determined to maximize sensitivity while minimizing damping losses. This study presents the first report on enhancing the sensitivity of the novel π-configuration SPR-based optical fibre sensor, uniquely designed to enable simultaneous multi-analyte sensing while significantly improving sensitivity through asymmetrical thin-film coating.

The proposed sensor has broad applications in medical diagnostics for the simultaneous detection of multiple biomarkers, environmental monitoring for real-time sensing of heavy metals and organic pollutants in water, chemical and gas sensing for the dual detection of volatile organic compounds (VOCs). By enabling multiplexed sensing in a single fibre, this work eliminates the need for complex sensor arrays while maintaining high sensitivity and low crosstalk. This work bridges a critical gap in SPR sensing by enabling simultaneous detection of two analytes without complex instrumentation, paving the way for next-generation biosensors. Future work will explore experimental validation and on-chip microfluidic integration.

2. Sensor Structural Design and Theoretical Simulations

2.1. Sensor Geometry and Material Configuration

The proposed π-configured optical fibre SPR sensor consists of a standard single-mode fibre (SMF-28, Corning) with two opposing side-polished regions to create dual sensing regions. This geometrical design was carried out using COMSOL Multiphysics software. It consists of a 3.1% GeO2 doped silica core with diameter 9 μm, and a pure silica cladding with diameter 125 μm. Figure 1a shows the 3D schematic diagram of the π-configuration SPR-based fibre optic sensor with dual sensing regions coated with metallic thin films. The proposed sensor can be fabricated through side-polishing technique (mechanical polishing) [17] or laser micro-machining [18]. This technique

 doi:10.20944/preprints202603.2389.v1

partially removes the cladding to expose the evanescent field while preserving the fibre's mechanical integrity, creating a flat polished surface that allows uniform deposition of plasmonic films and dielectric layers. The amount of residual cladding, D for each of the sensing regions is 0.7 μm from the core of the fibre. This has been carefully optimized to maximize evanescent field interaction while minimizing leakage losses. Magnetron sputtering or thermal evaporation techniques are utilized for the plasmonic thin-film deposition on the dual planar sensing regions [19,20]. The width $\boldsymbol{w}$, of the plasmonic sensing regions were optimized at 10 μm, while the thicknesses $\boldsymbol{t_m}$ and $\boldsymbol{t_t}$, of the metallic thin-film and titanium dioxide dielectric respectively were optimized at 45 nm and 10 nm respectively [15]. The 2D π-configuration dual SPR-based fibre optic sensor with the design parameters is illustrated in Figure 1b.

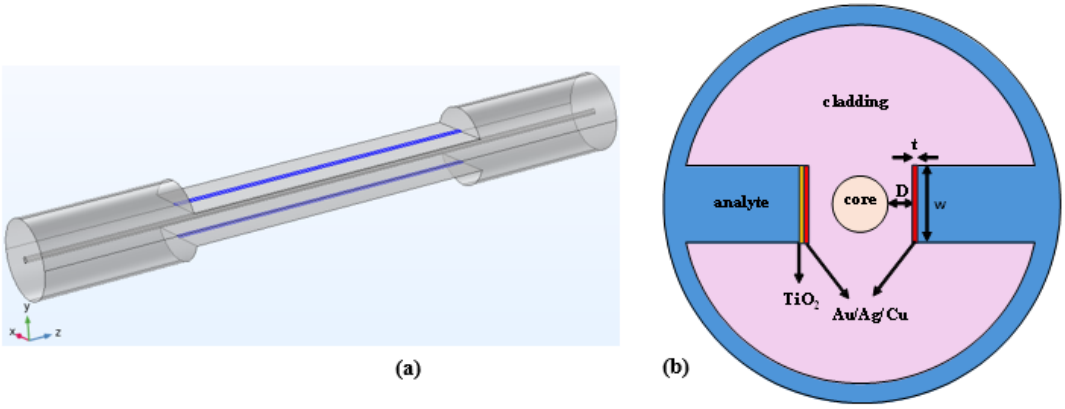

Figure 1. (a) 3D schematic of π-configuration SPR sensor; **(b)** sensor design in 2D.

2.2. Simulation Setup

The numerical simulations were conducted using COMSOL Multiphysics 6.3, employing the wave optics module to solve Maxwell's equations under the electromagnetic waves frequency-domain (ewfd) analysis. The computational domain consists of the fibre core, cladding, metallic thin films (Ag, Au, Cu), and dielectric (TiO2) modelled using experimentally validated Drude-Lorentz dispersion relations, operating wavelength of 600 – 1200 nm, and analyte region with refractive indices ranging from 1.37 to 1.42.

A perfectly matched layer (PML) was incorporated at the boundaries of the simulated region to eliminate unwanted reflections of any incident waves. The meshing strategy employed a physics-controlled extra-fine triangular mesh, refined at metal-analyte interfaces to accurately capture plasmonic wave propagation. For an experimental setup of π-configured dual SPR fibre optic sensor, the analyte flow mechanism is crucial for repeatable and reliable measurements. The π-configured sensor is embedded in a microfluidic flow cell with narrow channels that allows controlled analyte flow directly over the exposed sensing regions. The flow cell could be made of glass or polydimethylsiloxane (PDMS), to ensure optical transparency for light coupling into the fibre [21]. A syringe pump can be used to inject the analyte at controlled speeds. A broadband light source such as tungsten-halogen lamp is then coupled into the fibre sensor, and a spectrometer which captures the transmission spectrum, analyzing the shift in SPR dip based on the analyte refractive index. For this research, the desired analytes are viruses, however, other analytes like bacteria, glucose, proteins, and heavy metals in solutions may be used. Analytes interact with the sensor by varying its refractive index at the sensor surface, which simulates the binding of biomolecules. As a result, molecular interactions can be simulated and the sensitivity of the sensor assessed. To evaluate the performance of the sensor, parameter studies are conducted under various operating conditions. The effects of varying wavelengths, refractive indices, and geometric parameters on the SPR response are investigated by sweeping through the range of wavelengths, refractive indices, and geometric

 doi:10.20944/preprints202603.2389.v1

parameters. By using simulations, the optimal sensor design and operational parameters can be identified.

In SPR-based fibre optic sensors, resonance occurs when the wavevector of the guided optical mode in the fibre matches the wavevector of SPs at the metal-dielectric interface, ensuring the efficient energy transfer from the incident light to the SPWs, leading to a characteristic dip in transmission. At this interface, SPs propagate with a wavevector $\boldsymbol{k_{SPP}}$, given by [22]:

$$\boldsymbol{k_{SPP}} = \frac{2\pi}{\lambda}\sqrt{\frac{\varepsilon_m \varepsilon_d}{\varepsilon_m + \varepsilon_d}} \quad (1)$$

where λ is the wavelength of incident light, $\boldsymbol{\varepsilon_m}$ and $\boldsymbol{\varepsilon_d}$ are permittivity of the metal thin film and the dielectric analyte respectively. The wavevector $\boldsymbol{k_{mode}}$ of the fundamental guided mode of an optical fibre is given as [23]:

$$\boldsymbol{k_{mode}} = \frac{2\pi}{\lambda}\boldsymbol{n_{eff}} \quad (2)$$

where $\boldsymbol{n_{eff}}$ is the effective index of the guided mode in the fibre. It depends on the fibre core, cladding, metal thin film layer, and is obtained by solving the wave equation for optical fibre modes. The phase matching condition requires that $\boldsymbol{k_{mode}} = \boldsymbol{k_{SPP}}$ for resonance to occur [24]. Thus,

$$\boldsymbol{n_{eff}} = \sqrt{\frac{\varepsilon_m \varepsilon_d}{\varepsilon_m + \varepsilon_d}} \quad (3)$$

Equation 3 determines the refractive index at which SPR occurs based on the fibre mode properties, metal thin film type, and analyte refractive index.

The refractive indices of the Ge doped core, and the silica cladding are determined by utilizing the Sellmeier equation [25]:

$$\boldsymbol{n^2(\lambda)} = \mathbf{1} + \frac{A_1\lambda^2}{\lambda^2 - B_1} + \frac{A_2\lambda^2}{\lambda^2 - B_2} + \frac{A_3\lambda^2}{\lambda^2 - B_3} \quad (4)$$

where λ is the wavelength of incident light in $\boldsymbol{\mu m}$, n is the fibre core or cladding wavelength-dependent refractive index, and $\boldsymbol{A_1}$, $\boldsymbol{A_2}$, $\boldsymbol{A_3}$, $\boldsymbol{B_1}$, $\boldsymbol{B_2}$, and $\boldsymbol{B_3}$ are Sellmeier's constants obtained from [25].

Using the Drude-Lorentz model, the metal thin film dielectric function is determined by the relation [26]:

$$\boldsymbol{\varepsilon_m(\omega)} = \boldsymbol{\varepsilon_\alpha} - \frac{\omega_P^2}{\omega^2 + i\gamma\omega} + \Delta\boldsymbol{\varepsilon_P}\frac{\Omega_P^2}{\Omega_P^2 - \omega^2 - i\boldsymbol{\Gamma_P}\omega} \quad (5)$$

Where $\boldsymbol{\omega_P}$ is the plasma frequency, $\boldsymbol{\varepsilon_\alpha}$ is the metal interband offset, γ is the damping coefficient, $\Delta\boldsymbol{\varepsilon_P}$ is the weighting coefficient, Ω_P is the oscillator strength, and $\boldsymbol{\Gamma_P}$ is the spectral width. The values of the Drude-Lorentz parameters for Ag, Au, and Cu are obtained from [27].

Considering a dielectric layer, $\boldsymbol{TiO_2}$ of thickness $\boldsymbol{t_d}$ and permittivity $\boldsymbol{\varepsilon_d}$ between the metal and analyte, where it is assumed that the metal is thick enough to be semi-infinite in the x direction, and field decays away from the interfaces. Approximating for a thin, high index dielectric, $\boldsymbol{TiO_2}$, we obtain the modified phase-matching condition governed by the implicit equation derived from the transverse resonance condition for the asymmetric three-layer structure given as [28]:

$$\boldsymbol{\kappa_d}\tanh(\boldsymbol{\kappa_d t_d}) = \frac{\varepsilon_d\left(\frac{\kappa_m}{\varepsilon_m}\right) + \varepsilon_a\left(\frac{\kappa_a}{\varepsilon_a}\right)}{1 + \frac{\varepsilon_a \kappa_m}{\varepsilon_m \kappa_a}} \quad (6)$$

where $\boldsymbol{\kappa_d}$ is the inverse of the transverse decay length in $\boldsymbol{TiO_2}$, tanh is a hyperbolic tangent that describes the confinement of field in thin dielectric layers, $\boldsymbol{\kappa_m}$ and $\boldsymbol{\kappa_a}$ are transverse wavevectors in the metal and analyte respectively, and $\boldsymbol{\varepsilon_a}$ is the permittivity of the analyte. The term on the RHS embodies the modification of the effective surface plasmons boundary conditions by the presence of the $\boldsymbol{TiO_2}$ layer, shifting the resonance relative to the metal-analyte interface.

The refractive index (n) of $\boldsymbol{TiO_2}$ can be calculated using the expression [29]:

$$\boldsymbol{n^2} = \mathbf{5.913} + \frac{0.2441}{\lambda^2 - 0.0803} \quad (7)$$

The transmission coefficient (T) provides crucial information about the interaction between the light and sensing medium over a range of wavelengths [30]. It is expressed as:

$$\boldsymbol{T} = \boldsymbol{exp}\left(\frac{4\pi}{\lambda}.\left(\boldsymbol{n_{eff}}\right)_{\boldsymbol{imag}}.\boldsymbol{L}\right) \quad (8)$$

 doi:10.20944/preprints202603.2389.v1

where $(n_{eff})_{imag}$ is the imaginary part of the effective refractive index and L is the sensing region length. In SPR sensors, sensitivity S is the shift in the resonance wavelength ($\Delta\lambda_{res}$) per unit change in the analyte refractive index (Δn_a). It is given as [31]:

$$S = \frac{\Delta\lambda_{res}}{\Delta n_a} \quad (9)$$

The figure of merit (FOM) is a crucial parameter that quantifies the sensor's ability to distinguish between different analyte RI based on the sharpness and depth of the transmission spectrum dip. Typically, it is expressed as [32]:

$$FOM = \frac{S}{FWHM} \quad (10)$$

FWHM is the full width at half maximum of the SPR resonance dip, and it is a measure of the sharpness of the resonance [33].

3. Results and Discussions

3.1. Comparing Sensitivities of π-Configuration and D-Shaped SPR Sensors

The electric field of SPR-based fibre optic sensing is advanced by leveraging identical metal thin-films in a dual-sensing-region π-configuration, which offers a unique advantage of isolating the geometric contribution to crosstalk (opposite-side polishing) from material effects. This provides a baseline for the different hybrid configurations as sensing regions. The sensitivity for the π-configuration sensor using the same metal (Ag-Ag, Au-Au, and Cu-Cu) on both sensing surfaces is compared to that of a D-shaped optical fibre SPR-based sensor. Table 1 shows the comparison of sensitivities of the proposed π-configured dual SPR sensor using same combination of Ag/Au/Cu metallic thin films and the D-shaped SPR sensor using Ag/Au/Cu thin films from recent literature [15].

Table 1. Comparison of sensitivities for π-configuration and D-shaped SPR sensors.

RI	Sensitivity (nm/RIU)					
	π-Configuration Dual SPR sensor			D-shaped SPR sensor		
	Ag-Ag	Au-Au	Cu-Cu	Ag	Au	Cu
1.37	-	-	-	-	-	-
1.38	3300	3300	3000	1500	3200	2200
1.39	4400	4300	3900	4200	4200	3700
1.40	5900	5600	5400	5800	5500	5300
1.41	8100	7900	7300	8000	7800	7200
1.42	12500	12400	11400	12300	12200	11300

At high RI (n_a = 1.42), sensitivity is primarily governed by metal-dielectric contrast, not fibre geometry. Since both sensors use identical metallic thin films (45 nm), their plasmonic responses are inherently similar. At n_a = 1.42, the evanescent field penetration depth (~200 nm for Ag) approaches its maximum interaction limit. The pi-configuration's second sensing zone adds minimal extra field overlapping with the analyte.

The key advantage of the π-configuration is the dual-peak multiplexing capability. Unlike a single D-shaped sensor with one resonance peak, the π-configuration generates two distinct peaks if asymmetric coatings are used such as metal vs. metal + dielectric. This enables the simultaneous detection of two analytes without crosstalk. Another advantage of the π-configuration is that opposite-side polishing minimizes evanescent field overlapping between zones. This reduces interference when detecting dissimilar analytes. Also, dual sensing points allow self-referencing, where one region monitors reference RI, and the other detects analyte. This helps to improve reliability in noisy environments such as temperature fluctuations.

 doi:10.20944/preprints202603.2389.v1

3.2. Investigating π-Configuration Sensor Using Bimetallic Asymmetry Material

The π-configuration, dual spatially separated sensing interface, provides a unique architectural opportunity for multi-analyte detection using bimetallic asymmetry material. This method uses noble metals' material-specific dispersion to generate unique plasmonic resonances from the two sensing regions of the π-configuration [34]. The first sensing region was functionalized with a 45 nm silver (Ag) film, whereas the second sensing region was functionalized with a 45 nm gold (Au) film. This is a bimetallic π-sensor with the plasmonic metal's complicated dielectric function, $\varepsilon_m(\omega)$, as the only variable between the regions.

The operating principle is based on the unique dispersion relations between Ag and Au SPP modes. Figure 2 shows the transmission spectrum of the phase match between the core and SPP modes of the bimetallic asymmetric π-configuration sensor at an analyte RI of 1.41. This gives the real part of the effective index $\left(Re\left(n_{eff}\right)\right)$ as a function of wavelength for the fibre core mode (HE_{11}) and the consequent hybridized SPP modes for each metal at an RI of 1.41. For this RI, the Ag-region has a resonant wavelength of 856 nm, while the Au-region has a larger resonant wavelength of 912 nm. The intrinsic spectral separation ($\Delta\lambda$ = 56 nm) creates a natural demultiplexing mechanism, allowing the two resonance dips to be resolved within a single transmission spectrum without complex optical filtering.

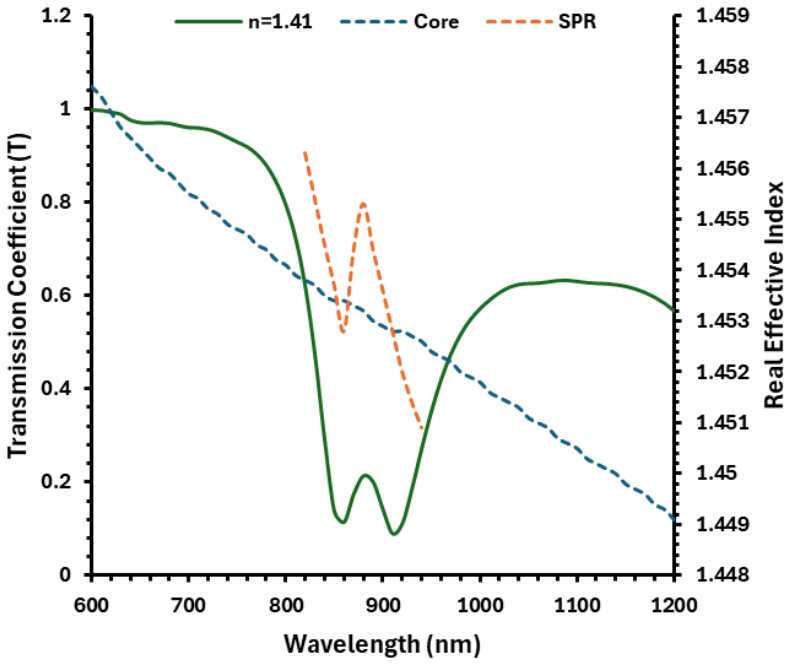

Figure 2. Phase matching between core and SPP modes of a bimetallic asymmetry π-configuration sensor.

The transmission spectra of the Ag/Au π-sensor were simulated for analytes with refractive indices ranging from 1.37 to 1.42. Figure 3 shows two clearly resolvable attenuation dips across the range, each exhibiting a linear redshift as the analyte RI increases. The first dip, with narrow width, is obtained from the interaction of light with Ag thin film, while the second peak, which is broader and shifts towards higher wavelengths, is obtained from the interaction of light with Au thin film. The sensitivity of each sensing region can be calculated by linearly regressing the resonance wavelength shift ($\Delta\lambda_{res}$) against the refractive index change (Δn_a). The Ag-region exhibited a

 doi:10.20944/preprints202603.2389.v1

sensitivity of 12700 nm/RIU, while the Au-region exhibited a lower sensitivity of 12200 nm/RIU. This is due to Au's broader resonance dip and more intrinsic loss. Crucially, the two sensitivities are orthogonal sensor outputs resulting from a single optical interrogation.

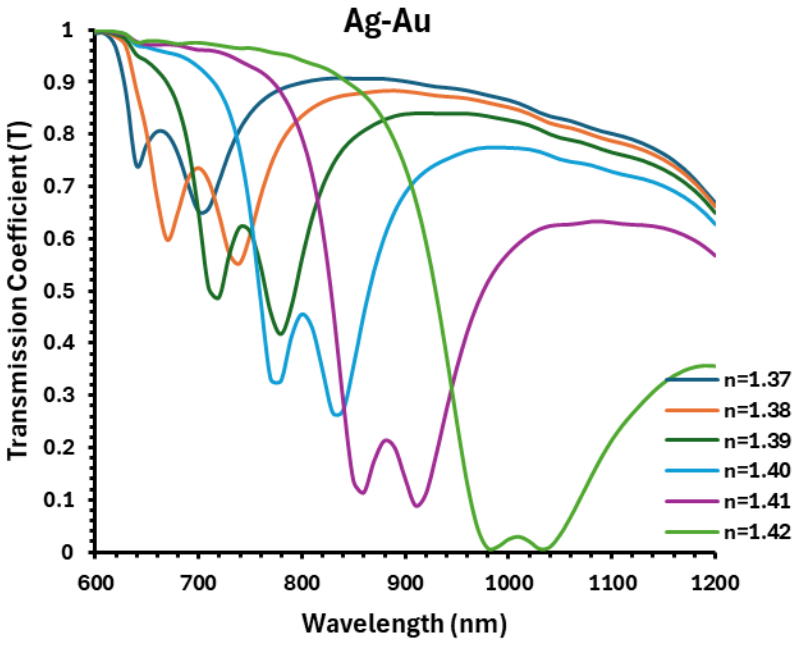

Figure 3. Transmission spectra for bimetallic asymmetric (Ag/Au) π-configuration sensor.

Figure 4 shows the plot of sensitivity against the analyte RI ranging from 1.37-1.42. The sensitivity obtained while varying the analyte RI are slightly greater when compared with the sensitivity of a single D-SPR gold or silver sensor for the same RI range (see Table 1).

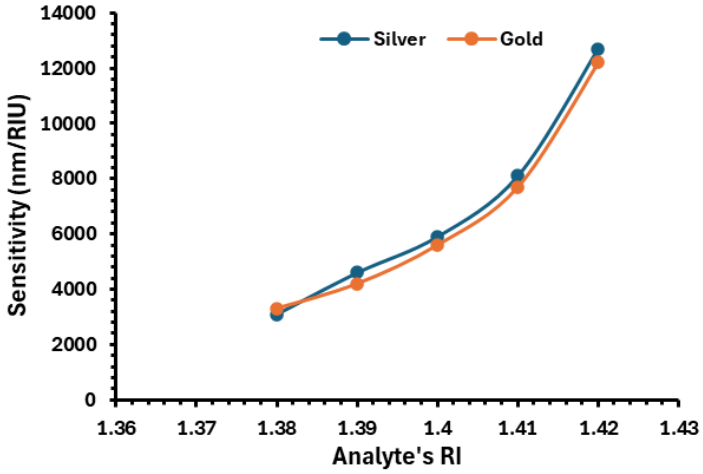

Figure 4. Plot of Sensitivity against RI of bimetallic asymmetry π-configured sensor.

This bimetallic asymmetry introduces material-dispersion encoded multiplexing, a new sensing paradigm. Unlike wavelength-division multiplexing, which uses separate light sources or complex grating structures [35], this method encodes multiple sensing regions into the device's inherent material properties. The two resonance wavelengths are fixed by design through metal selection, and their independent shifts offer two simultaneous measurements of the surrounding dielectric environment. This investigation reveals that the π-configuration is not just a dual-channel sensor, but also an integrated photonic sensor where strategic material asymmetry translates into spectrally resolved, multi-parameter output. It establishes the underlying proof that the design can accommodate independent sensing regions.

 doi:10.20944/preprints202603.2389.v1

3.3. Investigating π-Configuration Dual SPR Sensor Using Metal and Metal-TiO_2 Layers

The transmission spectrum of the π-configuration dual SPR sensor serves as the primary diagnostic tool for evaluating its performance, revealing critical insights into the plasmonic coupling efficiency at each sensing zone, and resonance peak separation ($\Delta\lambda$) for multi-analyte detection. This section combines theoretical modelling, finite-element simulations, and performance benchmarks to derive the spectral response of the dual-zone sensor using coupled-mode theory, quantify resonance wavelengths (λ_{spr}) and sensitivities for Ag and Ag-TiO_2 films, and compare results with conventional single D-shaped SPR sensors. TiO_2 is a high-refractive-index dielectric with unique optoelectronic properties that enhance SPR performance by increasing evanescent field confinement at the metal-dielectric interface, boosting sensitivity. It is inert to oxidation and biofouling and improves mechanical durability of metal thin films as an adhesive layer. The essence of using TiO_2 in π-configuration dual SPR sensing is to ensure spectral peak separation of the dips, enabling wavelength-division multiplexing (WDM). Figure 5 shows the transmission spectra for the metal and metal-TiO_2 sensing regions. The transmission spectrum for Ag & Ag-TiO_2 sensing regions is shown in figure 5a, while Au & Au-TiO_2, and Cu & Cu-TiO_2 sensing regions are shown in figure 5b and 5c respectively.

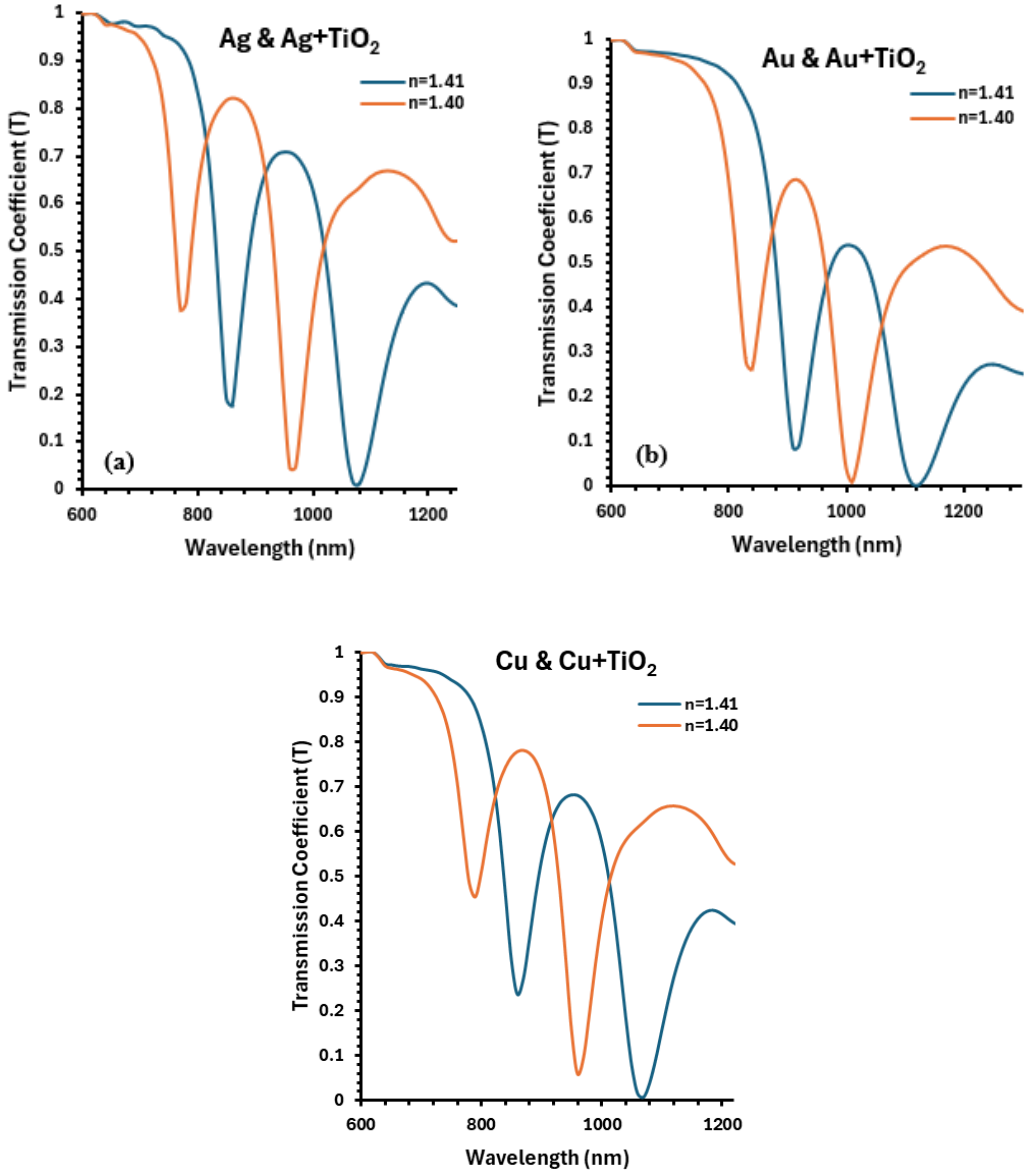

Figure 5. Transmission spectra for (a) Ag & Ag + TiO_2; (b) Au & Au + TiO_2; and (c) Cu & Cu + TiO_2 sensing regions.

 doi:10.20944/preprints202603.2389.v1

The metal/TiO_2-analyte interface generates stronger spectral shift than metal-analyte, increasing sensitivity. TiO_2's lower loss coefficient minimizes plasmonic damping, reducing interference between zones. The metal thin film's high plasmonic efficiency and TiO_2 RI engineering yields an optimized dual-region performance. Figure 6 illustrates the simulated electric field intensity distribution at the metal-dielectric and metal-TiO_2-dielectric interfaces of the π-configuration dual SPR optical fibre sensor. Figures 6a, b, c and d show the Ag-region SPR mode, Ag-region core mode, Ag + TiO_2-region SPR mode, and Ag + TiO_2-region core mode respectively. The figures confirm that two plasmonic modes are supported at the metal-analyte and metal-TiO_2-analyte interfaces, which contribute to two distinct dips in the transmission spectrum.

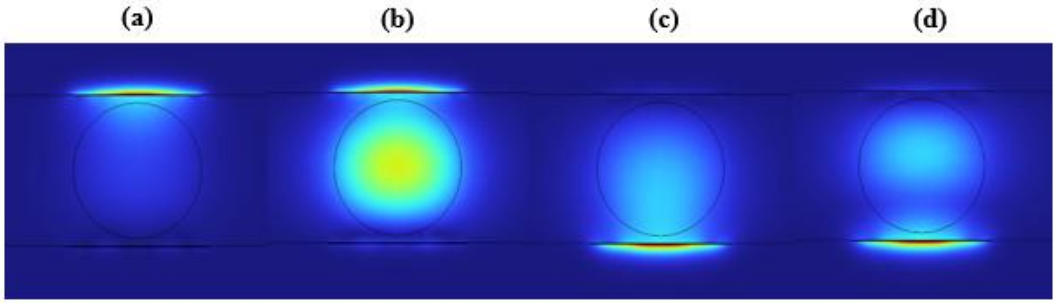

Figure 6. Electric field distribution for (a) Ag-region SPR mode; (b) Ag-region core mode; (c) Ag + TiO_2-region SPR mode; and (d) Ag + TiO_2-region core mode.

The metal-TiO_2 sensing region exhibits a longer red shift compared to the Ag-only zone due to increased effective refractive index (n_{eff}). TiO_2 has a high RI (n ≈ 2.4–2.6) compared to the analyte (n = 1.37–1.42). When deposited on the metal thin film, TiO_2 displaces the lower RI analyte near the metal surface, increasing the local n_{eff} at the plasmonic interface. The SPR evanescent field penetrates further into the TiO_2 layer due to its higher n, causing increased field to overlap with the analyte and reduced plasmon momentum, requiring lower-energy (longer λ) photons for resonance.

Figure 7 shows the wavelength sensitivity graph of the π-configuration dual SPR fibre optic sensor against the analyte RI. Figure 7a, 7b, and 7c show the sensitivity graph for Ag & Ag-TiO_2, Au & Au-TiO_2, and Cu & Cu-TiO_2 sensing regions respectively.

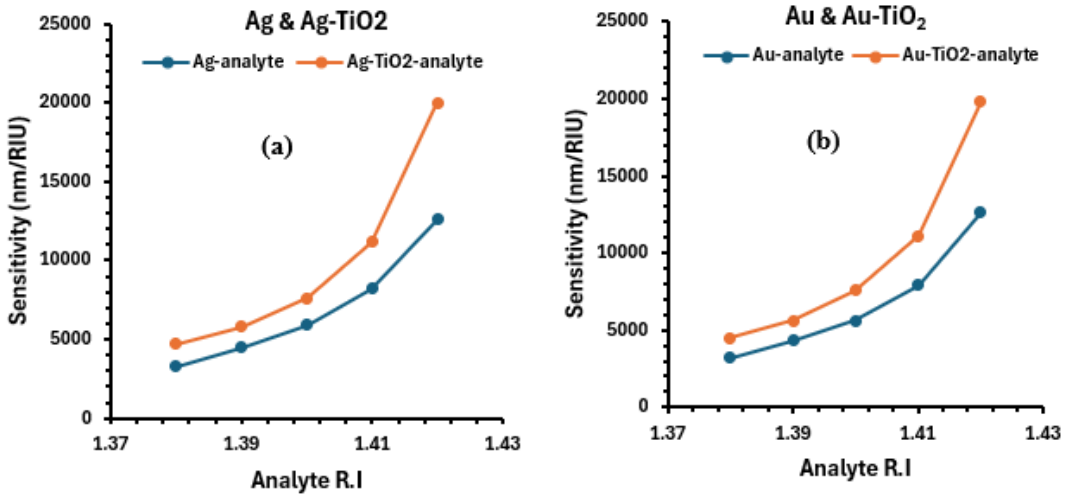

 doi:10.20944/preprints202603.2389.v1

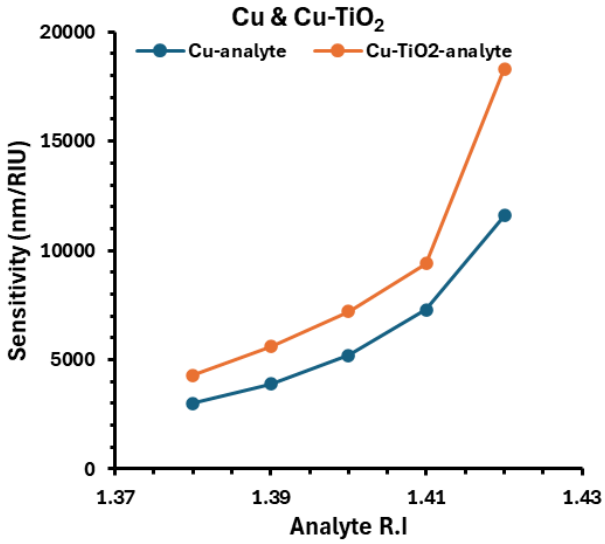

Figure 7. Wavelength sensitivity graph of **(a)** Ag & Ag-TiO_2; **(b)** Au & Au-TiO_2; and **(c)** Cu & Cu-TiO_2 sensing regions.

From graph 7a, silver and silver-TiO_2 π-configuration dual sensors have the highest wavelength sensitivities of 12,600 nmRIU-1 and 20,000 nmRIU-1 respectively at analyte RI of 1.42. Gold and gold-TiO_2 sensors have wavelength sensitivities of 12,600 nmRIU-1 and 19800 nmRIU-1 respectively, while copper and copper-TiO_2 sensors have wavelength sensitivities of 11,600 nmRIU-1 and 18,300 nmRIU-1 respectively for the same analyte RI. Silver had a slightly better sensitivity compared to gold due to the high plasma frequency, low optical losses, and better dielectric interactions. Silver has a high negative real permittivity (ε') which enhances field confinement, and a low imaginary permittivity (ε'') which reduces damping and minimizes losses, yielding deeper resonance dips and higher RI sensitivity. Ag-TiO_2 further enhances the field due to TiO_2's high refractive index (n ≈ 2.6), which increases the effective RI contrast, thereby reducing quenching of plasmons. Gold exhibits broader resonance due to interband transitions but at higher refractive indices and wavelengths (NIR), it has stronger negative real permittivity and lower imaginary part, minimizing losses. Copper exhibits higher losses due to oxidation and defects but still find application where cost implication is a factor. Figures 8a and 8b are the graphs of FWHM against the analyte RI for metal-metal and metal-metal/TiO_2 sensors respectively. FWHM is the spectral width of an SPR peak at half its maximum intensity. A narrower FWHM indicates a sharper resonance peak, leading to higher resolution in detecting small RI changes. A broader FWHM reduces resolution because small spectral shifts become harder to distinguish from noise [36]. Ag-Ag clearly showed a smaller FWHM compared to Au-Au and Cu-Cu for the metal-metal sensing regions, while Ag-Ag/TiO_2 showed a smaller FWHM at higher RI compared to Au-Au/TiO_2 and Cu-Cu/TiO_2 regions, indicating a sharper resonance dip. For the π-configuration sensor with distinct peaks, a narrow FWHM helps to clearly resolve them. An overlap in broad peaks due to large FWHM can merge, reducing the ability to distinguish between two analytes or sensing regions.

 doi:10.20944/preprints202603.2389.v1

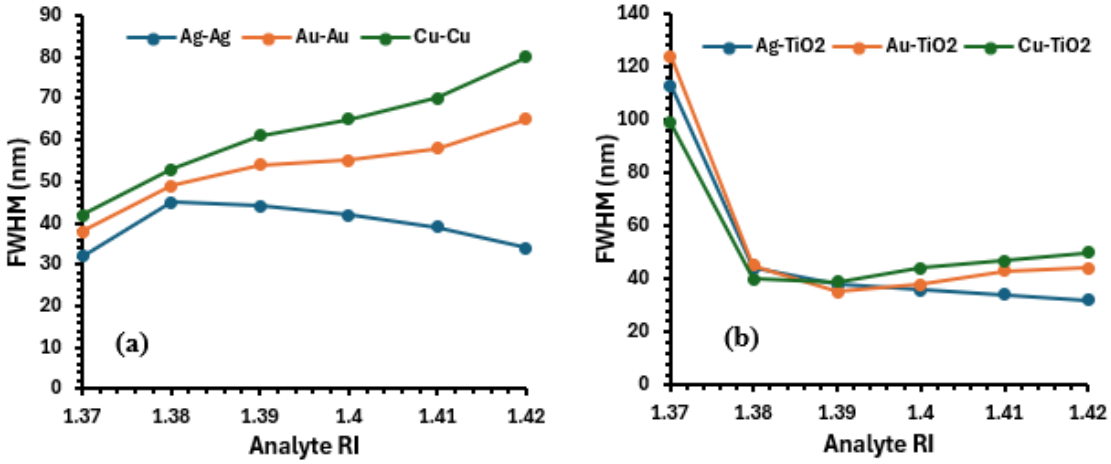

Figure 8. FWHM against RI graph of (a) metal-metal regions; and (b) metal-metal/TiO_2 regions.

Table 2 shows the comparison in the difference between the metal-analyte peak wavelength ($\Delta\lambda_{SPR1}$) and the metal-TiO_2-analyte peak wavelength ($\Delta\lambda_{SPR2}$).

Table 2. Spectral Separation for π-configuration metal-TiO_2 sensors.

Analyte RI	**Peak Wavelength Separation ($\Delta\lambda_{SPR}$) for metal-TiO₂ sensor (nm)**		
	Ag-TiO₂	Au-TiO₂	Cu-TiO₂
1.42	294	277	272
1.41	220	205	205
1.40	190	173	174
1.39	173	153	156
1.38	160	140	141
1.37	146	127	128

In the π-configuration dual SPR sensor, the spectral separation ($\Delta\lambda_{SPR}$) between the resonance dips of the two sensing zones is critical for enabling multi-analyte detection, minimizing potential crosstalk, and optimizing sensitivity. The ability to resolve two distinct peaks depends on material-induced shifts and coupling conditions. A sufficiently large $\Delta\lambda_{SPR}$ ensures that each peak can be independently tracked for RI changes in two different analytes.

The Rayleigh Criterion states that two peaks are resolvable if $\Delta\lambda_{SPR}$ ≥ FWHM (Full Width at Half Maximum) of the narrower peak [37]. If $\Delta\lambda_{SPR}$ is too small (<50 nm), the evanescent field overlaps between zones causes peak merging (loss of dual-analyte capability) and inaccurate sensitivity calculations (apparent shift ≠ true RI change). For this sensor design, $\Delta\lambda_{SPR}$ > 125 nm was achieved for all refractive index range (n = 1.37 – 1.42), thereby minimizing potential crosstalk and ensuring each peak in the spectrum is easily identified. Table 3 shows a comparison of the novel π-configuration SPR-based optical fibre sensor utilizing metal + metal/TiO_2 thin films with existing designs reported in literature.

 doi:10.20944/preprints202603.2389.v1

Table 3. Comparison of the π-configuration SPR-based optical fibre sensor with existing sensors reported in literature.

Ref	Sensor configuration	Sensing material	RI range	Wavelength sensitivity (nm/RIU)	FOM	Resolution (RIU^{-1})
[38]	Dual-core D-shaped PCF	Silver	1.35-1.5	3,400	-	$2.94x10^{-5}$
[39]	Dual-symmetrical D-shaped	Gold	1.21-1.22	5,000	-	-
[40]	Dual-channel PCF	Gold	1.33-1.40	11,600	-	$8.62x10^{-6}$
[41]	Dual-core D-shaped	Gold	1.33-1.44	17,000	320	$5.88x10^{-6}$
	π-config SPR	Silver	1.37-1.42	12,600	394	$7.94x10^{-6}$
This work	π-config SPR	Ag/TiO_2	1.37-1.42	20,000	625	$5.0x10^{-6}$

4. Conclusions

This study successfully designed, modelled, and characterized a novel π-configuration dual SPR sensor based on a single D-shaped optical fibre with opposing side-polished regions functionalized with Ag/Au/Cu and Ag/Au/Cu-$\boldsymbol{TiO_2}$ thin films. Through comprehensive finite-element simulations using COMSOL Multiphysics and theoretical analysis, we demonstrated that this architecture enables high-sensitivity, multi-analyte detection while minimizing crosstalk between sensing zones, a critical limitation in conventional SPR designs.

The investigation of the π-configuration sensor featuring a bimetallic asymmetry (Ag/Au) design produced two resolvable resonance dips, at 983 nm (Ag) and 1034 nm (Au), with sensitivities of 12700 nm/RIU and 12200 nm/RIU respectively for an analyte RI of 1.42. The integration of metal-dielectric (Ag-$\boldsymbol{TiO_2}$) in one sensing region induced a significant red shift of 294 nm (982 nm vs. 1276 nm), enabling wavelength-division multiplexing (WDM) for simultaneous dual-analyte detection. $\boldsymbol{TiO_2}$'s high refractive index (n ≈ 2.6) enhanced the local evanescent field, boosting sensitivity from 12,600 nm/RIU in the Ag-analyte region to 20,000 nm/RIU in Ag-TiO2-analyte region. $\boldsymbol{TiO_2}$ coating further improved stability by mitigating Ag oxidation, a key advantage over Cu-based sensors. The >125 nm peak separation resolved two distinct analytes eliminating the need for complex multi-core fibres or sensor arrays, reducing system cost and complexity.

This work establishes the π-configuration dual SPR sensor as a compact, high-performance platform for multiplexed sensing, addressing key limitations of traditional SPR systems. By combining geometric innovation, hybrid material engineering, and crosstalk-optimized design, this research opens new avenues for next-generation optical biosensors in healthcare, environmental monitoring, and industrial applications. This research design has potential for real-time, label-free monitoring of biomarkers, and multiplexed detection of heavy metals or organic pollutants in water. Future works includes the experimental validation of the sensor in real biofluid samples, integration with microfluidics for lab-on-a-chip applications, and exploration of 2D materials such as graphene or MoS_2 for further sensitivity enhancement.

Author Contributions: Conceptualization, J.E., R.P., and S.K.; methodology, J.E., and R.P.; software, J.E., R.P., and S.K.; investigation, J.E., R.P., and S.K.; data curation, J.E., and R.P.; writing—original draft preparation, J.E.; writing—review and editing, R.P., and S.K.; visualization, J.E., R.P., and S.K.; supervision, R.P., and S.K. All authors have read and agreed to the published version of the manuscript.

 doi:10.20944/preprints202603.2389.v1

Funding: This research received no external funding.

Institutional Review Board Statement: Not applicable.

Informed Consent Statement: Not applicable.

Data Availability Statement: The data supporting the findings of this study are available from the corresponding author upon reasonable request.

References

1. S. Das, R. Devireddy and M. R. Gartia, "Surface plasmon resonance (SPR) sensor for cancer biomarker detection," Biosensors, vol. 13, (3), pp. 396, 2023.
2. P. Berini, "Long-range surface plasmon polaritons," Advances in Optics and Photonics, vol. 1, (3), pp. 484–588, 2009.
3. A. Philip and A. R. Kumar, "The performance enhancement of surface plasmon resonance optical sensors using nanomaterials: A review," Coord. Chem. Rev., vol. 458, pp. 214424, 2022.
4. J. Johny, S. Amos and R. Prabhu, "Optical fibre-based sensors for oil and gas applications," Sensors, vol. 21, (18), pp. 6047, 2021.
5. K. Bhavsar et al, "Fibre optic sensor to detect heavy metal pollutants in water environments," in OCEANS 2017-Aberdeen, 2017,
6. Y. Xu et al, "Recent developments in micro-structured fiber optic sensors," Fibers, vol. 5, (1), pp. 3, 2017.
7. J. Jing et al, "Performance improvement approaches for optical fiber SPR sensors and their sensing applications," Photonics Research, vol. 10, (1), pp. 126–147, 2021.
8. J. Homola et al, "Multi-analyte surface plasmon resonance biosensing," Methods, vol. 37, (1), pp. 26–36, 2005.
9. G. Marusov et al, "A microarray biosensor for multiplexed detection of microbes using grating-coupled surface plasmon resonance imaging," Environ. Sci. Technol., vol. 46, (1), pp. 348–359, 2012.
10. W. Lin et al, "Cladding mode fitting-assisted automatic refractive index demodulation optical fiber sensor probe based on tilted fiber bragg grating and SPR," Sensors, vol. 22, (8), pp. 3032, 2022.
11. A. Klenke et al, "High-power multicore fiber laser systems," Progress in Quantum Electronics, vol. 84, pp. 100412, 2022.
12. R. G. Sanedrin et al, "Seed-mediated growth of bimetallic prisms," Adv Mater, vol. 17, (8), pp. 1027–1031, 2005.
13. J. Ehiabhili, R. Prabhu and S. Kannan, "Design and numerical analysis of an ultra-sensitive π-configuration fibre optic-based SPR sensor: Dual plasmonic enhancement for low-refractive-index biomolecular detection," in Photonics, 2026,
14. M. A. Abbas et al, "Engineering multimodal dielectric resonance of TiO2 based nanostructures for high-performance refractive index sensing applications," Optics Express, vol. 28, (16), pp. 23509–23522, 2020.
15. J. Ehiabhili, R. Prabhu and S. Kannan, "Highly sensitive D-SPR sensors with optimized metallic thin films for bio-analyte detection," in Photonics, 2024,
16. S. K. Dubey et al, "A study of highly sensitive D-shaped optical fiber surface plasmon resonance based refractive index sensor using grating structures of Ag-TiO2 and Ag-SnO2," Optik, vol. 252, pp. 168527, 2022.
17. S. Tseng and C. Chen, "Side-polished fibers," Appl. Opt., vol. 31, (18), pp. 3438–3447, 1992.
18. Y. Yu et al, "Ultra-short pulsed laser manufacturing and surface processing of microdevices," Engineering, vol. 4, (6), pp. 779–786, 2018.
19. R. Garg et al, "Sputtering thin films: Materials, applications, challenges and future directions," Adv. Colloid Interface Sci., pp. 103203, 2024.
20. T. Del Rosso et al, "Accurate and simultaneous measurement of thickness and refractive index of thermally evaporated thin organic films by surface plasmon resonance spectroscopy," Optics Express, vol. 22, (16), pp. 18914–18923, 2014.
21. A. K. Pathak et al, "Investigation of a SPR based refractive index sensor using a single mode fiber with a large D shaped microfluidic channel," OSA Continuum, vol. 2, (11), pp. 3008–3018, 2019.

 doi:10.20944/preprints202603.2389.v1

22. Y. Ying et al, "Determination of refractive index using surface plasmon resonance (SPR) and rigorous coupled wave analysis (RCWA) with a D-shaped optical fiber and a nano-gold grating," Instrum Sci Technol, vol. 48, (4), pp. 376–385, 2020.
23. M. D. Feit and J. A. Fleck Jr, "Computation of mode properties in optical fiber waveguides by a propagating beam method," Appl. Opt., vol. 19, (7), pp. 1154–1164, 1980.
24. Z. Han and S. I. Bozhevolnyi, "Radiation guiding with surface plasmon polaritons," Reports on Progress in Physics, vol. 76, (1), pp. 016402, 2012.
25. H. N. Rafi, M. R. Kaysir and M. J. Islam, "Air-hole attributed performance of photonic crystal fiber-based SPR sensors," Sensing and Bio-Sensing Research, vol. 29, pp. 100364, 2020.
26. D. Rioux et al, "An analytic model for the dielectric function of Au, Ag, and their alloys," Advanced Optical Materials, vol. 2, (2), pp. 176–182, 2014.
27. V. G. Kravets, P. Y. Kurioz and L. V. Poperenko, "Spectral dependence of the magnetic modulation of surface plasmon polaritons in permalloy/noble metal films," Josa B, vol. 31, (8), pp. 1836–1844, 2014.
28. Z. Han and S. I. Bozhevolnyi, "Radiation guiding with surface plasmon polaritons," Reports on Progress in Physics, vol. 76, (1), pp. 016402, 2012.
29. P. Tao et al, "TiO 2 nanocomposites with high refractive index and transparency," Journal of Materials Chemistry, vol. 21, (46), pp. 18623–18629, 2011.
30. A. Shalabney and I. Abdulhalim, "Sensitivity-enhancement methods for surface plasmon sensors," Laser & Photonics Reviews, vol. 5, (4), pp. 571–606, 2011.
31. R. A. Kadhim et al, "Highly sensitive D-shaped optical fiber surface plasmon resonance refractive index sensor based on Ag-α-Fe 2 O 3 grating," IEEE Sensors Journal, vol. 20, (17), pp. 9816–9824, 2020.
32. A. K. Mishra, S. K. Mishra and B. D. Gupta, "SPR based fiber optic sensor for refractive index sensing with enhanced detection accuracy and figure of merit in visible region," Opt. Commun., vol. 344, pp. 86–91, 2015.
33. E. Kazuma and T. Tatsuma, "Localized surface plasmon resonance sensors based on wavelength-tunable spectral dips," Nanoscale, vol. 6, (4), pp. 2397–2405, 2014.
34. A. Agrawal, R. W. Johns and D. J. Milliron, "Control of localized surface plasmon resonances in metal oxide nanocrystals," Annual Review of Materials Research, vol. 47, (1), pp. 1–31, 2017.
35. K. Grobe and M. Eiselt, Wavelength Division Multiplexing: A Practical Engineering Guide. 2013.
36. E. Nahid et al, "Au-strip structure dependent performance investigation of D-shaped SPR sensors for biosensing applications," Results in Optics, vol. 12, pp. 100460, 2023.
37. K. A. Willets et al, "Super-resolution imaging and plasmonics," Chem. Rev., vol. 117, (11), pp. 7538–7582, 2017.
38. S. Chu et al, "A surface plasmon resonance biosensor based on dual core D-shaped photonic crystal fibre embedded with silver nanowires for multisensing," IEEE Sensors Journal, vol. 21, (1), pp. 76–84, 2020.
39. S. Osamah et al, "Study of single and symmetrical D-shaped optical fiber sensor based on gold nanorods," Journal of Optics, vol. 52, (4), pp. 2048–2058, 2023.
40. P. Bing et al, "Analysis of dual-channel simultaneous detection of photonic crystal fiber sensors," Plasmonics, vol. 15, (4), pp. 1071–1076, 2020.
41. M. Momtaj et al, "Open-channel-based dual-core D-shaped photonic crystal fiber plasmonic biosensor," Appl. Opt., vol. 59, (28), pp. 8856–8865, 2020.